Microfluid Nanofluid (2013) 14:785–795
DOI 10.1007/s10404-012-1096-2

Droplets coalescence and mixing with identical and distinct surface tension on a wettability gradient surface

Szu-I Yeh · Wei-Feng Fang · Horn-Jiunn Sheen · Jing-Tang Yang

Received: 29 August 2012 / Accepted: 5 November 2012 / Published online: 21 November 2012

Abstract The influence of identical and distinct surface tensions on the coalescence and mixing of droplets after a direct collision on a wettability gradient surface (made from a self-assembled monolayer, SAM technique) was investigated. The results indicate that their mixing is driven sequentially by interior convection and diffusion; the convection endures less than 100 ms but dominates more than 60 % of the mixing. If the stationary droplet has a large surface tension (73.28 mN × m^{-1}), whether the moving droplet has a large surface tension (73.28 mN × m^{-1}) or a small surface tension (38.63 mN × m^{-1}), the mushroom-shaped mixing pattern is generated within the coalesced droplet that enhances the convective mixing and also significantly enlarges the interface for mass diffusion. The mixing index of these two cases was greater than 0.8 at 120 s after the collision. For the cases in which the stationary droplet with a small surface tension collided by the moving droplet with a large surface tension, a mixing pattern with a round-head shape developed, which was insufficient to benefit the mixing. When the stationary and moving droplets both had small surface tension, the moving droplet was unable to merge with stationary droplet and had poor mixing quality due to the small surface Gibbs energy of both stationary and moving droplets. For the collision of droplets of identical surface tension, the surface tension affects the coalescence behavior; for the collision of droplets with distinct surface tension, the coalescence behavior and mixing quality depend on the colliding arrangement of stationary and moving droplets.

Keywords Surface tension · Droplets coalescence · Microfluidic mixing · μ-PIV · μ-LIF

S.-I. Yeh · H.-J. Sheen
Institute of Applied Mechanics, National Taiwan University, 1 Sec. 4 Roosevelt Rd., Taipei 106, Taiwan

W.-F. Fang · J.-T. Yang (✉)
Department of Mechanical Engineering, National Taiwan University, 1 Sec. 4 Roosevelt Rd., Taipei 106, Taiwan
e-mail: jtyang@ntu.edu.tw

1 Introduction

Droplet-based microfluidic systems have attracted much attention for their prospective applications in optics, electronics, and lab-on-a-chip (LOC). They are expected to revolutionize biological laboratory procedures by allowing assays more rapid and free of error, in which the droplets carry biological samples. Transport, collision and mixing of droplets are the key issues in the development of droplet-based microfluidic systems (Huebner et al. 2008; Fouillet et al. 2008; Fair 2007).

Various techniques to manipulate a droplet have been proposed, including electrowetting on a dielectric (EWOD) (Cho et al. 2003; Baviere et al. 2008), a light-driven method (Ichimura et al. 2000) and a thermal gradient (Darhuber et al. 2003). These approaches regarded as active means require an external source to drive the droplet: EWOD uses a high driving voltage that might induce side effects in bio-applications; the thermal-gradient method also has problems of biocompatibility due to the high temperature exerted; the transport velocity of a droplet driven by light (about 0.03 mm/s) is less than that with other methods. A passive means, as an alternative to enable droplet movement, that has been developed for several years uses chemical or mechanical modification of a surface to form on it a wettability gradient, along which a droplet is able to transport spontaneously without external power, thus without undesirable side effect. Several

surface-modified methods such as microstructural fabrication (Yang et al. 2006, 2009), deposition of a thin polymer film (Ruardy et al. 1997), and SAM techniques (Choi et al. 2012; Chaudhury and Whitesides 1992) served to fabricate surfaces with wettability gradients. Lai et al. (2010a) fabricated a silicon surface with a combination of structure and SAM gradients that achieved a droplet moving about 9 mm along the surface.

A collision between droplets is an important feature of various applications, such as spray combustion, polymer blending and petrochemical manufacture. The angle, velocity and distance between colliding droplets cause three modes of droplet collision: coalescence, partial coalescence and bounce. Two dimensionless parameters—Weber number ($We = 2R\rho U_r^2/\gamma$, with droplet radius R, relative velocity U_r, density ρ and surface tension γ of the liquid) and impact number ($B = X/(r_1 + r_2)$, with distance X between the centers of mass of two droplets of radii r_1 and r_2; $B = 0$ signifies a direct collision)—are related to modes of droplet collision. Orme (1997) presented a map relating these three modes and the two parameters. Of these modes, droplet coalescence is the most important because of its applications in microfluidic systems for biochemical reactions in which mixing of reagents and samples become the primary definitive step. Sellier and Trelluyer (2009) hence used a simple scenario to describe the coalescence of sessile droplets and confirmed the power-law growth of the neck between the droplets. Danov et al. (1993) applied a theoretical approach to the deformation of emulsion droplets before and after their coalescence; their numerical calculations investigated the distance over which the droplet deforms and the total force acting between the droplets. Eggers et al. (1999) presented the general case of droplet coalescence on a flat surface with numerical calculations; their results predict a transition between regimes dominated by a capillary–viscous balance and by a capillary–inertia balance.

The mixing of biochemical regents in a microfluidic device is a critical step to improve the practicability of a μTAS (micro total analysis system) or LOC. Fluid mixing under the condition of this small size relies mainly on molecular diffusion and chaotic advection. Several methods to increase the mixing efficiency in continuous flow systems are reported, such as increasing the contact surface between the two fluids (Fang and Yang 2009) and creating chaotic flow patterns within the fluid (Stroock et al. 2002). Researchers have tried to manipulate discrete droplets to achieve a rapid mixing of fluids (Hosokawa et al. 1999) through the internal motions of fluids caused by the rapid release of the interfacial force during the droplet coalescence or by the shear interaction with surroundings. The merged droplet is, however, typically not well mixed in a few seconds. EWOD-based devices have been developed to mix rapidly the merged droplet, accelerated through active manipulation of the droplets by linear electrodes and a varied aspect ratio of the droplets (Paik et al. 2003).

Several researchers investigated the morphology and dynamics of droplet collision and coalescence in plane surface or in microchannel using plane-film and simulation tool (Chesters 1991; Kapur and Gaskell 2007; Jose and Cubaud 2012). Extensive effort has been undertaken to reveal the mixing mechanisms inside droplets. The traditional dye methods showed the color change due to mixing of two coalesced droplets, and micro-particle-image velocimetry (micro-PIV) showed the recirculation field inside a moving droplet in a straight (Wang et al. 2007) or winding microchannel (Tung et al. 2009). These methods were used also to observe the mixing of two fluids in a coalesced droplet in EWOD devices; the results showed that two symmetric circulations existed within the droplet (Lu et al. 2008). Kinoshita et al. (2007) applied confocal micro-PIV to obtain velocity information inside a droplet moving in a microchannel. Longmire and his research group applied dual-field high-speed PIV (Kim and Longmire 2009) and tomographic PIV (Ortiz-Duenas et al. 2010) to study the collisions of droplets in silicon oil; their trajectories and the small-scale motion within droplets with varied Weber number and collision angle were resolved. This experiment yielded profound insight into the flow physics in droplet collisions and coalescence on a flat surface. Lai et al. (2010b) utilized PIV and a confocal microscope to measure the coalescence, internal flows, and mixing patterns of droplets. During the period of coalescence, the released surface energy of the droplets created a pair recirculation flow inside the merged droplet so as to improve the fluid mixing. Castrejon-Pita et al. (2011) also used micro-PIV to investigate the internal flow in the glycerol/water droplets during impact and coalescence.

Most droplet-based mixers have so far consisted of either microchannels or electrowetting devices that are alien to an open system; tests of the phenomena of droplets mixing on an open microfluidics system are little addressed. The surface tension that varies widely for biochemical reagents might be the main factors to influence droplet collision and the mixing of fluids. How surface tension affects droplet coalescence and mixing behavior is also little addressed. In this work, we used droplets with identical and distinct surface tensions to perform collision, coalescence and mixing of binary droplets on a surface with a wettability gradient. Micro-PIV and measurements of confocal fluorescence disclosed the internal flow and 3D mixing patterns of two droplets on merging on a surface with a wettability gradient. We demonstrated that for

droplets with identical surface tension, a larger surface tension caused stronger recirculation flow in a coalesced droplet; for droplets with distinct surface tensions, the coalescence and mixing behavior were dominated by the arrangement of the two droplets. Our experimental results can serve as a basis for applications of droplet-based μTAS or LOC systems.

2 Experiments

2.1 Preparation of a gradient surface

With a modified vapor-diffusion self-assembled monolayer (SAM) method, we fabricated a surface with a wettability gradient on a plain glass microscope slide so that the light of μPIV and μLIF and their signals can transmit through from the bottom. This substrate can also avoid optical distortion caused by the curved surface of a droplet that constitutes a main problem for quantitative visualization of the flow field within liquid droplets on open systems. The clean glass slide was placed vertically in a bottle containing decyltrichlorosilane (DTS) solution (0.025 %, dissolved in dry toluene). The saturated SAM was formed on the region immersed in the DTS solution. The other region above the liquid surface of the solution has a wettability gradient because DTS vapor diffused and deposited on the substrate. This immersion lasted 15 min.

The wettability gradient of the surfaces was characterized on measuring the static contact angles (θ) along the surface with a sessile-drop method and a commercial contact-angle meter (OCA 20, Dataphysics Instruments, Germany). The contact angle of water on this surface varied from 105° to 55° at a distance within 0.4 mm. The maximum difference of contact angle between two separate surfaces is less than ±2.5° for the region of liquid immersion and less than ±6.5° for the region of vapor diffusion. The stability of the SAM gradient was tested; no obvious degradation was observed after transporting 50 deionized (DI) water droplets. Further details of fabrication of the gradient surface and measurement of the contact angle are reported previously (Lai et al. 2010a).

2.2 Working fluids

To produce fluids with varied surface tension, we used a surfactant (Tween 20®, polyoxyethylene sorbitan monolaurate, Pierce Chemical Co.) that decreased the surface tension of a fluid when added to DI water. The surface tension of DI water is 73.28 mN/m; we added the surfactant (0.001 %) to DI water to alter the surface tension to 38.63 mN/m. The surface tension was measured with a surface tensiometer (EZ-Pi, Kibron Inc. Helsinki, Finland). The critical micelle concentration (CMC) of Tween 20® is 60 mg/L. In our study, the volume concentration of surfactant (Tween 20®) we used to lower down the surface tension does not exceed the CMC value. Therefore, there is no micelle to affect the coalescence-induced flow. The nonuniform distribution of the surfactant on the surface of a moving droplet might cause the Marangoni effect that induces the interfacial flow between two droplets. Several researchers explored the relationship between surfactant distribution and the droplets coalescence in the presence of Marangoni stresses (Blanchette et al. 2009; Lu and Corvalan 2012). In this study, we focused only on the variation of internal flow and the mixing patterns of colliding droplets with identical and distinct surface tensions.

The contact angles of two working fluids on the slides are listed in Table 1. The maximum difference of contact angle between two separate surfaces is less than ±1.7° for the region of liquid immersion and less than ±6.3° for the region of vapor diffusion. The contact angles for the two working fluids were 47.5° and 51.2°, respectively.

2.3 Apparatus

The experimental apparatus is sketched in Fig. 1. A commercial confocal microscope system (Nikon A1R), designed to avoid affecting the flow patterns by the surrounding disturbance, was used to observe the droplet on the surface with a wettability gradient. Droplets generated with a syringe pump (KDS220, KD Scientific) and microliter syringes (Hamilton 710RN) had volume 300 ± 12 nL. One droplet was laid on the hydrophilic region of the surface, called a stationary droplet; afterward, the other droplet (moving droplet) was dropped on the hydrophobic region of the surface so that it moved spontaneously to collide with the stationary droplet through being driven by the wettability gradient (from a hydrophobic to a hydrophilic region). The platform to control the points of droplet falling was a motorized *xyz* positioning stage. The working fluids used in four experimental cases are listed in Table 1. The droplets in cases A and B have identical surface tension; the droplets in cases C and D have distinct surface tensions.

The high-speed camera (IDT X-stream) with an objective lens captured the views at a rate 1,000 fps and resolution 2,352 × 1,782 pixels (2.1 × 1.6 mm) for the μ-PIV measurement and calculation. The field of view (FOV) was about 1.2 × 1.2 mm (512 × 512 pixels) corresponding to a spatial resolution 2.34 μm per pixel. The axial resolution of the system was approximately 5 μm. μPIV was used to investigate the internal flow induced from the coalescence of a droplet. Seeding particles (polystyrene particles, Duke Scientific) of diameter 1 μm and density 1.05 g/cm^3 were added to the working fluids. The images captured with the

Table 1 Surface tensions and contact angles on the hydrophilic (glass substrate) and hydrophobic regions (a hydrophobic SAM layer on the substrate) of two working fluids, and our experimental cases

	Surface tension (mN m^{-1})	At hydrophobic region (°)	At hydrophilic region (°)
Working fluids			
Working fluid A	73.28	106.7	59.2
Working fluid B	38.63	71.6	20.4
	Stationary droplet		Moving droplet
Experimental cases			
Case A	Working fluid A		Working fluid A
Case B	Working fluid B		Working fluid B
Case C	Working fluid A		Working fluid B
Case D	Working fluid B		Working fluid A

high-speed camera were processed with a standard cross-correlation scheme (Insight 5, TSI Inc.) to produce the raw vector field. This scheme implemented a multi-pass interrogation in which in the first-pass, cross-correlation was calculated for an interrogation spot of area 64 × 64 pixels; the interrogation spot was then divided into four subareas 32 × 32 pixels for the second-pass calculation. The interrogation spots overlapped by half; a Gaussian fit was used to resolve the sub-pixel displacement. The upper limit of the μPIV measurement, determined by the size of the interrogation spots, was about 43 mm/s. Each experimental case was performed 20 times and the reproducibility of the results is more than 95 %.

2.4 Microfluorescence

The mixing efficiency and mixing pattern inside the coalesced droplet were measured with a laser and a microfluorescence (μ-LIF) technique. Fluorescent DNA solutions of FAM-labeled oligonucleotide (6-carboxy-fluorescein, 2 μM, 495/521 nm) and Cy-5-labeled oligonucleotide (cyanine dye, 2 μM, 646/662 nm) were adopted to simulate the mixing of biochemical fluids. The light for excitation, provided from an argon-ion laser (488 nm) or a diode laser (638 nm), was directed into an objective lens (plane apochromat VC ×10, NA = 0.45) with a dichroic mirror, with which the excitation light and emitted light were separated. A pinhole (diameter 12.8 μm) was installed behind the dichroic mirror to exclude optically the light from an out-of-focus plane. The intensity of the emitted light was measured with two separate photomultiplier tubes (PMT) behind the filter blocks. The thickness of the optical slice in this setup was less than 11 μm; the field of view was about 1.2 × 1.2 mm. Using a *xyz* stage to scan several *z*-positions, we viewed the 3D reconstructed distribution of fluids through the great vertical resolution of the confocal microscope.

3 Results and discussion

3.1 Flow patterns and mixing patterns within a droplet

We investigated the coalescence behaviors of direct ("head-on") collisions between a moving and stationary droplet on a wettability gradient surface. The moving droplet that was placed on the edge of a DTS-saturated region transported spontaneously. The droplet diameters and related dimensionless parameters of these working fluids are listed in Table 2. The Weber number (We, ratio of inertial force to surface tension force) is about 10^{-3} to 10^{-5}, i.e., much smaller than unity, which means that two droplets are expected to coalesce (Orme 1997), and the coalescence of the droplets is little affected by the transport velocity of the moving droplet. The ratio of surface tension to gravity is given by the Bond number, Bo; for all working

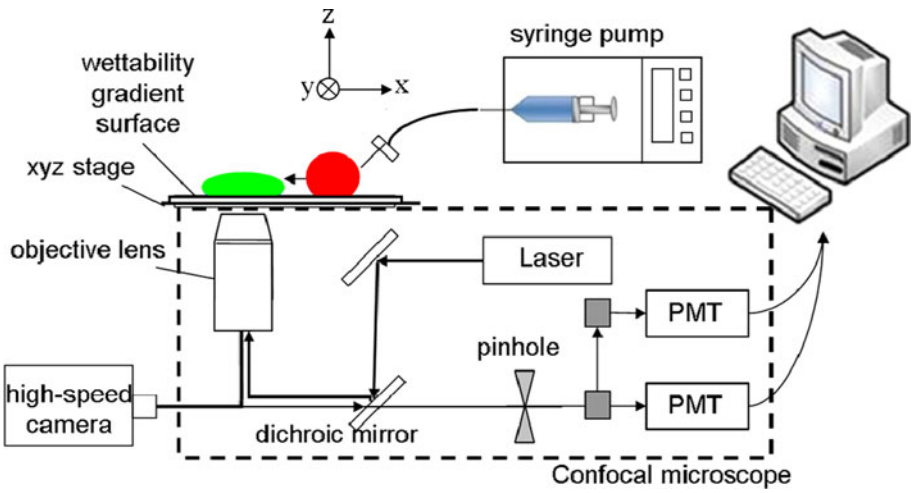

Fig. 1 Schematic diagram of the experiment. The μPIV images were recorded with a high-speed camera; the 3D mixing patterns were recorded with the confocal laser-scanning microscope

Table 2 Properties, droplet size in various regions, dimensionless parameters and average transport velocity of working fluids A and B

Working fluid	Viscosity (cP)	Surface tension (mN/m)	Radius 1 (μm)	Radius 2 (μm)	We	Bo	Transport velocity (mm/s)
A	1.13	73.28	536.5 ± 2.5	354.5 ± 3.0	2.28×10^{-3}	7.95×10^{-9}	15.4
B	1.11	38.63	747.5 ± 4.5	442.5 ± 3.5	5.84×10^{-4}	2.09×10^{-8}	5.1

Diameters 1 and 2 denote the droplet diameter (0.2 μL) on hydrophilic (without DTS) and hydrophobic (saturated DTS) regions, respectively

fluids, the corresponding Bo on each region of the surface is much less than unity (10^{-8} to 10^{-9}). Surface tension hence plays an important role in coalescence that affects the mixing efficiency of the droplets after collision. The average transport velocity of the moving droplet before collision was determined on tracking its center, also listed in Table 2.

The energy released during the coalescence is evaluated by the change of Gibbs energy G, which for a droplet of radius R on a substrate, is expressed as.

$$G = 2\pi R^2(1 - \cos\theta)\gamma - \pi(R\sin\theta)^2\gamma\cos\theta \quad (1)$$

According to this equation, the differences of Gibbs energy between two droplets (both of volume 0.2 μL) and a coalesced droplet for working fluids A and B are estimated to be 0.070 and 0.024 μJ, respectively. For all working fluids, less than 0.1 % surface energy is transferred to kinetic energy; the remaining surface energy is released mostly during coalescence of the droplets, thus producing deformation and vibration of the droplets.

We utilized a μPIV system to measure the flow field inside a droplet during coalescence after the collision of the droplets. We made cross-sectional measurements at three focal positions—bottom, middle and top of the coalesced droplet. As the flow patterns were similar at the three focal positions, the velocity fields were analyzed only at the middle of the droplet ($z = 60$ μm). We defined $t = 0$ as the instant of contact of the two droplets in all experimental cases.

According to the velocity fields inside the droplets, the mixing occurs in two stages: an initial rapid (<100 ms) spread of molecules through convective mass transfer (*convection period*) with a large average speed ($\sim$1.0 mm/s) inside the droplet, and a slow redistribution of molecules through diffusion (*diffusive period*) with a small average speed (<0.1 mm/s). For all experimental cases, the average speed decreased to less than 0.1 mm/s within 100 ms. The mixing patterns of biochemical molecules (fluorescently labeled oligonucleotides) in droplets with varied viscosity or surface tension were measured with the μLIF technique. Ten slices of a coalesced droplet were captured along the z-axis with an interval 10–15 μm (depending on the size of the droplet) to resolve the 3D mixing patterns inside the droplet. The confocal system completed a planar scanning (a slice) in 30.5 ms (512 × 512 pixels) but required about 10 s to scan completely a 3D mixing pattern. As the mixing of droplets through convective mass transfer sustains less than 1 s after the droplets collide, this confocal system was unable to track the 3D mixing patterns during the convection. When the mixing was dominated by diffusion, the patterns altered slowly; we thus obtained a 3D mixing pattern approximately 6–8 s after collision of the droplets (the early diffusion-dominated process), which is analogous to that at the end of the convection. The 2D mixing patterns of the droplets at $z = 60$ μm for the various fluids are shown in Figs. 2–5; the 3D mixing patterns for the various fluids captured approximately 6–8 s after collision of the droplets were reconstructed, as shown also in Figs. 2–5. The green fluorescence signifies the fluid with FAM from the stationary droplet, whereas the red fluorescence signifies that with Cy-5 from the moving droplet.

The velocity fields in droplets during coalescence for experimental cases A–D at $z = 60$ μm are shown in Figs. 2–5. For experimental case A, a flow from right to left in the x-direction was observed at $t = 2$ ms, and a pair of symmetric vortices (recirculation flows) were subsequently formed at $t = 12$ ms and sustained to $t = 40$ ms, shown in Fig 2a. Afterward, the internal energy was too weak to sustain the symmetric vortices; the internal flow inside the coalesced droplet became oscillatory as shown in Fig. 2b,c. The 2D and 3D mixing pattern was generated by the vortices during the convection period, displaying a mushroom shape, as shown in Fig. 2d. The fluid in the stationary droplet was squeezed spirally toward the side. After this occurrence, the fluids spread vertically and horizontally, resulting in an enhanced subsequent diffusive mass transfer in the diffusion period.

For experimental case B, a central flow from right to left caused by the moving droplet was observed at the right side of the coalesced droplet and sustained more than 20 ms. Because of the small surface tension (weak cohesive forces) of the droplets, the moving droplet was unable to penetrate, and to be surrounded by, the stationary droplet. For this case, the amount of surface Gibbs energy of the system was smaller than that for other cases, which represents that the internal energy incurred by the collision was small; the vortices in the coalesced droplet were consequently weak and dissipated quickly. At $t = 22$ ms,

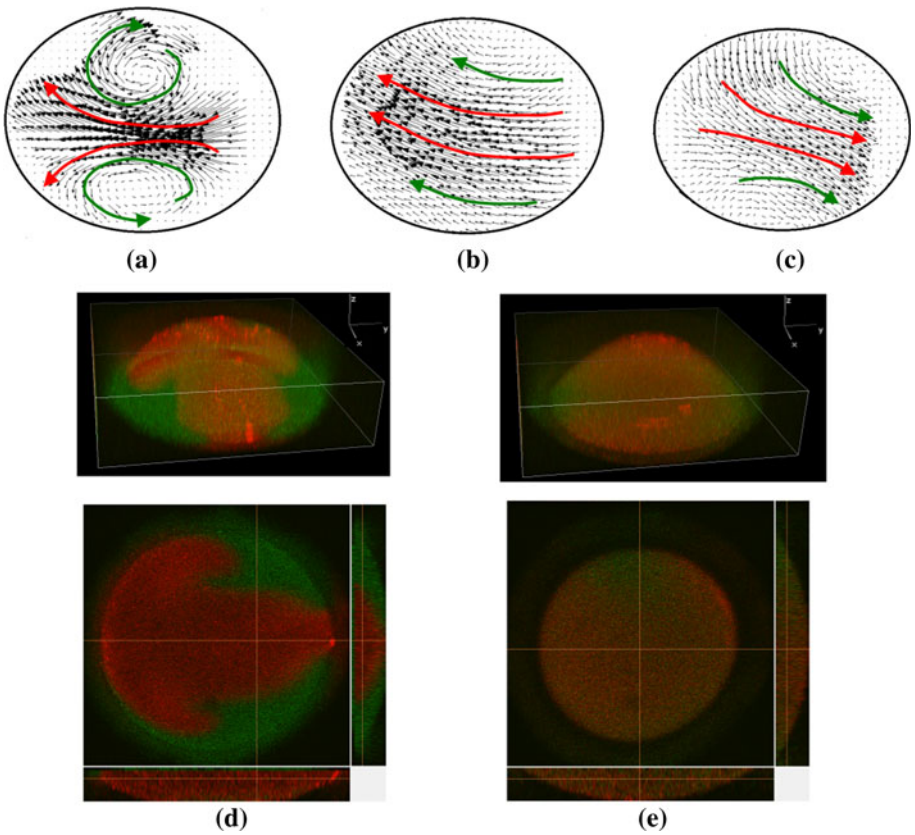

Fig. 2 **a–c** Velocity vectors of the internal flow of case A at $t = 12$, 42 and 46 ms respectively after droplet collision. **d** Reconstructed 3D distribution of case A at $t = 10.35$ s and the slices view at $z = 60$ μm, $t = 2.22$ s. **e** Reconstructed 3D distribution of case A at $t = 98.47$ s and the slices view at $z = 60$ μm, $t = 95.62$ s. *Green* indicates the fluid from the stationary droplet whereas *red* indicates the fluid from the moving droplet. z-axis is 200 % zoomed for the 3D figures

the internal flow of the coalesced droplet generated oscillation as shown in Fig. 3b, c. For this case, a portion of the moving droplet was unmerged with the stationary droplet even over 120 s after the droplet collision (see Fig. 3d, e). Of the moving droplets, 40–50 % by volume was unable to merge into a stationary droplet for experimental case B.

The flow patterns for case C were analogous to that for case A, showing strong recirculation flows inside the coalesced droplet. The internal flow moved from the right to the left side of the droplet, and then spread along the boundary. A pair of symmetric recirculation flow subsequently formed and sustained at $t = 6$–30 ms as shown in Fig. 4a. After $t = 32$ ms, the internal energy gradually dissipated, leading to flow from right to left in the center declining, and resulting in the symmetric recirculation flow becoming unsustainable (see Fig. 4b). The internal flow therefore oscillated as shown in Fig. 4c. Because the surface tensions of the stationary and moving droplets for cases A and C were different, leading to the corresponding different total surface Gibbs energy, the strength and duration of vortices were dissimilar, which is addressed in the following section. The mixing patterns for case C are approximately complementary to that for case A, which means the fluid of stationary droplet formed a mushroom-shaped distribution similar to the distribution of the moving droplet in case A, but the scenarios of formation of the flow patterns in these two cases differ. For case A, the stationary droplet was squeezed by the collision of the moving droplet and formed vortices that induced the mushroom-shaped mixing pattern occurring in the moving droplet, whereas for case C, because of the surface tension (cohesion force) of the stationary droplet being larger than that of the moving droplet, the moving droplet was enclosed and squeezed by the stationary droplet, forming the mushroom-shaped mixing pattern.

The stationary droplet in the case D has a smaller surface Gibbs energy than the stationary droplet in case A; the recirculation flow in the coalesced droplet was consequently much weaker and sustained for a briefer duration (Fig. 5a). Afterward, the oscillation flow in the droplet appeared at $t = 20$ ms and sustained about 60 ms as shown in Fig. 5b, c. The mixing pattern illustrates that the fluid of the moving droplet was surrounded by the fluid of the stationary droplet as shown in Fig. 5d. As the surface tension (cohesive force) of the moving droplet was larger than that of the stationary droplet, the moving droplet was little deformed (i.e., prone to retain a spherical shape) by the effect of the stationary droplet, and therefore formed a round-head shape inside the stationary droplet.

In all experimental cases, we depicted the mixing patterns through the corresponding flow patterns, concluding that the mixing patterns were caused by the initial rapid spread of molecules through the convective mass transfer (the period of convection was less than 40 ms), and the subsequent oscillatory flow was unlikely effective in the mixing

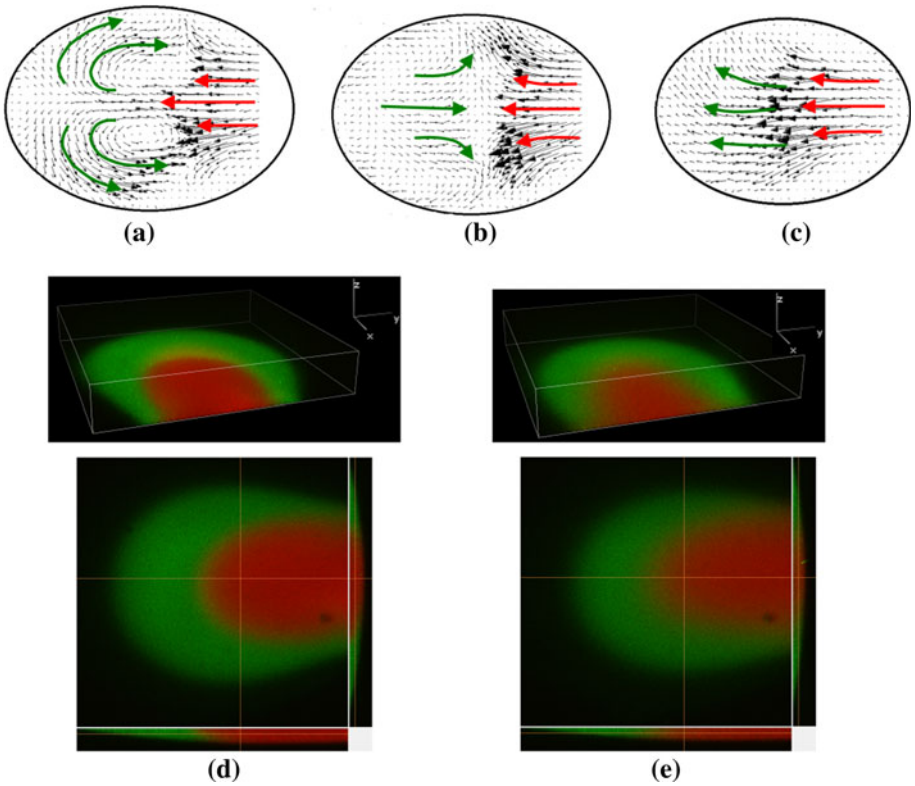

Fig. 3 **a–c** Velocity vectors of the internal flow of case B at $t = 14$, 24 and 26 ms respectively after the droplet collision. **d** Reconstructed 3D distribution of case B at $t = 10.24$ s and the slices view at $z = 30$ μm, $t = 4.55$ s. **e** Reconstructed 3D distribution of case B at $t = 98.52$ s and the slices view at $z = 30$ μm, $t = 94.41$ s. *Green marks* the fluid from the stationary droplet whereas *red* indicates the fluid from the moving droplet. z-axis is 200 % zoomed for the 3D figures

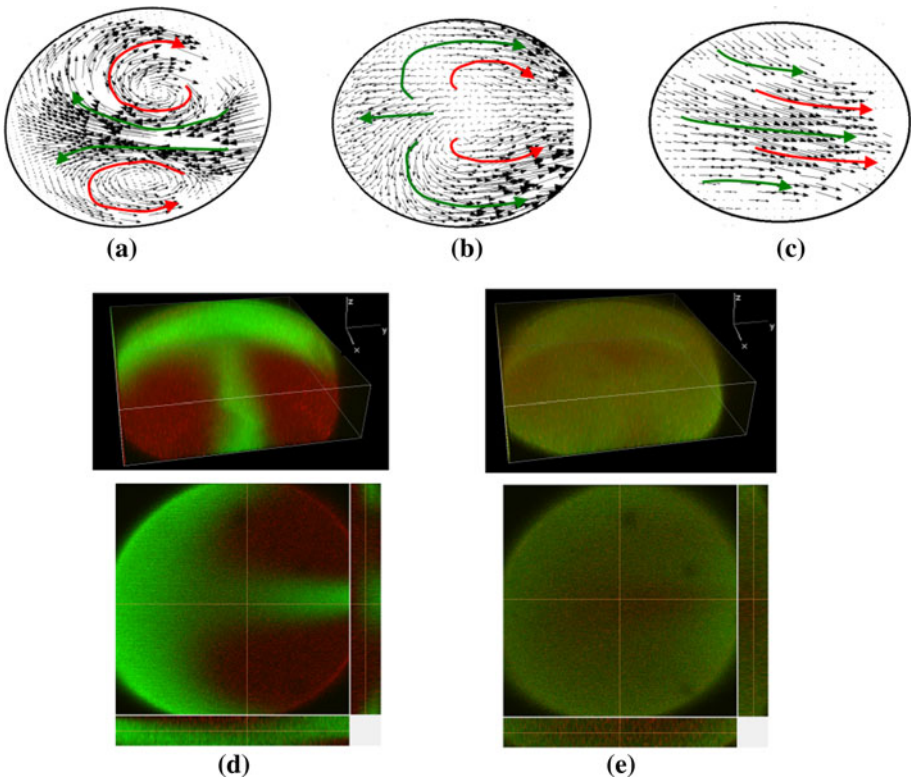

Fig. 4 **a–c** Velocity vectors of internal flow of case C at $t = 6$, 32 and 36 ms respectively after droplet collision. **d** Reconstructed 3D distribution of case C at $t = 8.91$ s and the slices view at $z = 60$ μm, $t = 2.70$ s. **e** Reconstructed 3D distribution of case C at $t = 95.78$ s and the slices view at $z = 60$ μm, $t = 92.83$ s. *Green marks* the fluid from the stationary droplet whereas *red* indicates the fluid from the moving droplet. z-axis is 200 % zoomed for the 3D figures

patterns. For all experimental cases, although there was a large velocity inside the coalesced droplet, the droplet was unable to slide on the surface because of restriction by the surface energy barrier. The energy was transferred from the moving droplet to the coalesced droplet, thus causing the internal flow field to vary in the coalesced droplet.

3.2 Quantitative analysis of the flow field and mixing efficiency

The recirculation disturbed the flow inside the coalesced droplet so as to enhance the droplet mixing during coalescence. We calculated the circulation inside the coalesced droplet for experimental cases A–D. For this calculation, we first defined an integral path that was a closed contour approximating to the boundary of zero vorticity of the concentration of a vortex identified in flow-velocity fields (Ting and Yang 2009). The overall vorticity/velocity gradient inside the coalesced droplet for all fluids decreased with the dissipation of the energy. Figure 6 shows the temporal circulation change of experimental cases A–D. The average circulations of experimental cases A–D were 3.23×10^{-6}, 2.05×10^{-6}, 3.58×10^{-6} and 1.87×10^{-6}m^2/s, respectively, the corresponding durations of vortex circulation were 32, 10, 26 and 12 ms, respectively.

The surface Gibbs energy of a droplet on hydrophilic and hydrophobic surfaces, and of a droplet on hydrophilic and hydrophobic surfaces are 0.0305, 0.1020, 0.0299 and 0.0248 μJ, respectively. For distinct droplet collisions (cases C and D), the greater discrepancy of the surface Gibbs energy between the moving and stationary droplet caused the flow interaction to become more efficient; the vortices occurred earlier than for the identical droplet collisions (cases A and B). For cases B and D, the smaller pulling force (smaller surface tension of the stationary droplet) during the droplet coalescence resulted in decreased circulation and duration of vortices. In contrast with cases B and D, the larger surface tension of the moving droplet (greater pulling force in the droplet coalescence) induced a stronger recirculation flow, larger circulation, and a greater duration of the vortices. For cases A and C, the flow patterns for case C were analogous to that for case A, showing strong recirculation flows inside the coalesced droplet.

The mixing index M_i commonly used to describe the mixing quality of fluids and the scale of fluid mixing is defined as.

$$M_i = 1 - \left(\frac{\int_V |C_{cy} - C_\infty| dV}{\int_V |C_0 - C_\infty| dV} \right) \quad (2)$$

in which C_{cy} is the 3D temporally dependent distribution of concentration of Cy-5-labeled oligonucleotide (red), C_0 and C_∞ are the concentrations of a fully unmixed droplet and a fully mixed droplet, respectively (Tung et al. 2009). In order to obtain C_0, we applied the μLIF measurement to a 0.4 μL fully unmixed droplet (i.e., contains Cy-5 only) that placed on the hydrophilic region of the gradient surface. The Cy-5 is uniformly dispersed inside the droplet so that the obtained intensities are not significantly varied with the position. We therefore assigned the spatial averaged intensity as the value of C_0. Similarly, C_∞ is obtained from the intensity measurement of a droplet in which the

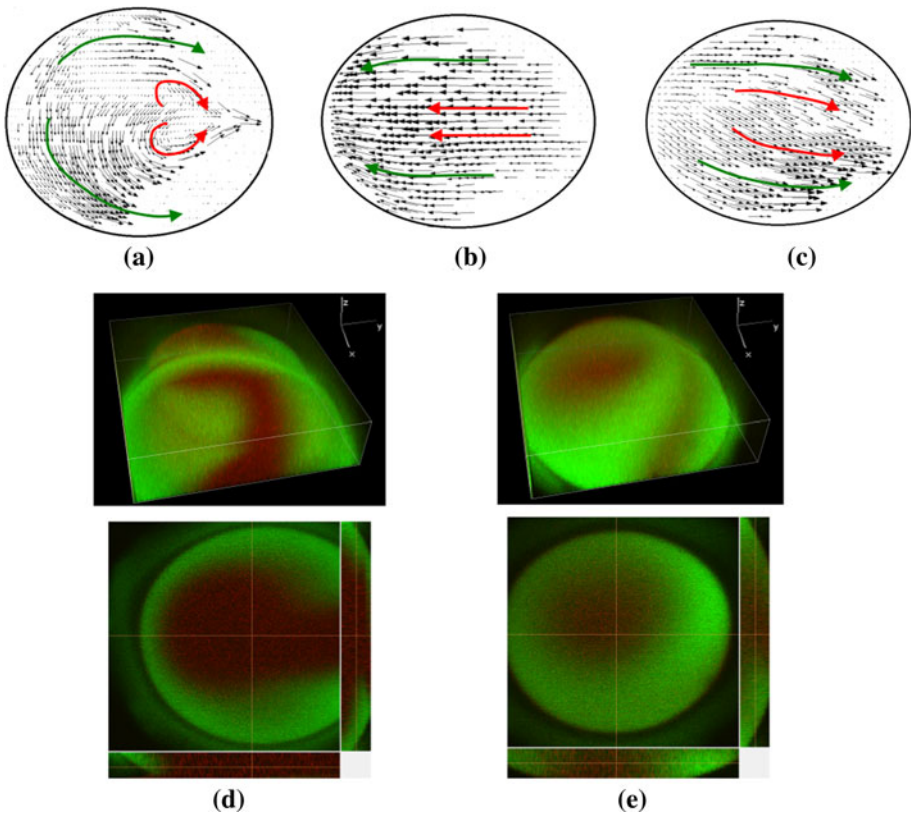

Fig. 5 **a–c** Velocity vectors of the internal flow of case D at $t = 8$, 20, 24 ms, respectively after the droplet collision. **d** Reconstructed 3D distribution of case D at $t = 10.45$ s and the slices view at $z = 60$ μm, $t = 2.71$ s. **e** Reconstructed 3D distribution of case D at $t = 97.75$ s and the slices view at $z = 60$ μm, $t = 93.76$ s. *Green marks* the fluid from the stationary droplet whereas *red* indicates the fluid from the moving droplet. z-axis is 200 % zoomed for the 3D figures

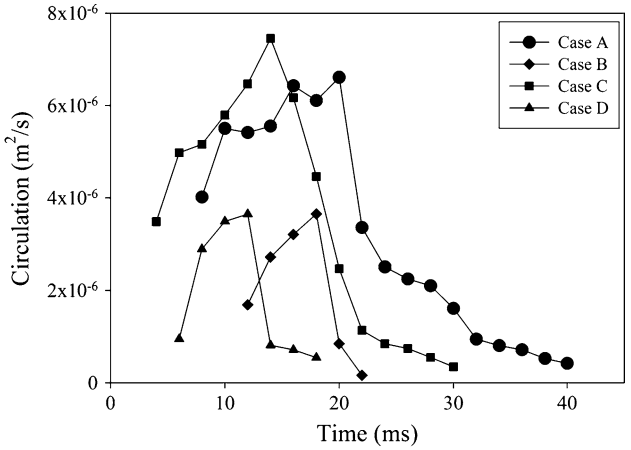

Fig. 6 Transient vortex circulation of experimental cases A–D

FAM and the Cy-5 are premixed. The mixing index of value unity means that fluids become fully mixed, whereas zero represents fluids entirely unmixed. The concentration distributions were evaluated from the distribution of light intensity of the μLIF measurement that was assumed to be proportional to the number density of the fluorescently labeled oligonucleotide. The mixing index was evaluated also from the concentration distributions of FAM; no significant difference was found.

The transient mixing indices of experimental cases A–D are shown in Fig. 7. As the confocal system took about 6–8 s to measure 15–20 planes, each data point represented the mixing index averaged over the 3D scanning duration. The mixing index was unavailable within a few seconds because the scanning rate was limited. For experimental case B, the part outside the field of view was assumed to be totally unmixed. The mixing indices of experimental cases A–D at 120 s after the collision of the droplets were 0.82, 0.42, 0.86 and 0.71, respectively. That the mixing indices of cases A and C are all larger than 0.8 means that mixing in these cases is effective. The mixing quality of fluids resulting from the recirculation flow for experimental cases A and C is demonstrated to benefit the mixing. The contact area or material interface of two fluids is the key factor for molecular diffusion. For experimental cases A and C, the larger material interface of a mushroom-shaped mixing pattern enhanced the mixing efficiency in diffusion-dominated mixing. For experimental cases B and D, the smaller material interface of the mixing pattern with a round-head shape failed to benefit the mixing. In particular, for case B, the droplets were not totally merged. Although the recirculation increased the contact area between the two separate fluids, the contact area of two different fluids was still less than in other cases. The mixing indexes of experimental case B at 120 s after collision of the droplets was 0.42, much smaller than that of the other experimental cases. A portion of the moving droplet was unmerged with the stationary droplet; the efficacy of the droplet mixing was therefore poor, rendering small mixing indices.

The measured data points were fitted to an exponentially decreasing function, $M_i = a + b(1 - e^{-ct})$, in which parameters a, b and c were evaluated by the least-squares method. Based on the regression curves, the mixing indices of experimental cases A–D were 0.52, 0.33, 0.62 and 0.46, respectively at $t = 100$ ms, during which the mixing of the droplets was dominated by convection. The slope ($\Delta M_i/\Delta t$, $\mathrm{d}M$) of the regression curves for experimental cases A–D indicates that $\mathrm{d}M_A \sim \mathrm{d}M_C > \mathrm{d}M_D > \mathrm{d}M_B$, which conforms to the range of the material interface. The flow recirculation influenced the droplet mixing at both convection-dominant and diffusion-dominant stages because it caused the extension of the contact area of the fluids in the merged droplet. Once the interfacial area of the fluids was extended, the mixing of the fluids was promoted. The slope of the mixing indices for experimental cases A, C and D is almost the same as, and steeper than, for experimental case B, demonstrating that the extended interface enhanced the diffusion for fluid mixing. The mixing indices of the droplets at $t = 100$ s for experimental cases A–D are 63.4, 78.6, 72.1 and 64.7 % of that at $t = 120$ s respectively, showing that more than 60 % of the entire mixing of the droplets occurred during the convection-dominant process. The mixing quality is hence mainly determined less than 100 ms after the droplet collision.

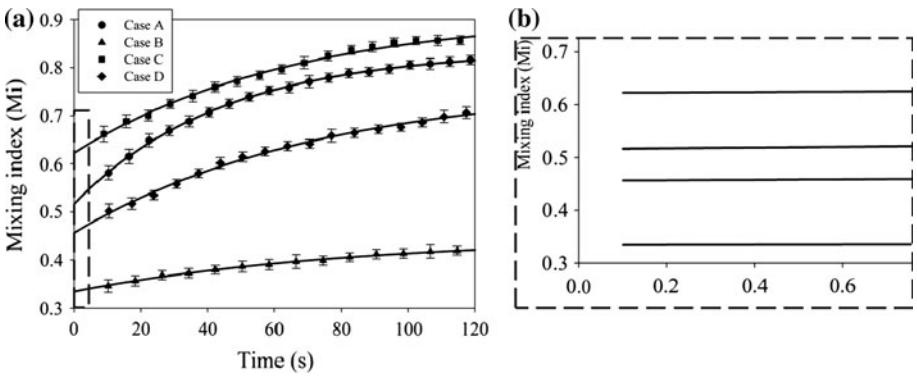

Fig. 7 **a** Transient mixing indices of experimental cases A–D and **b** the *magnified figure* from the *rectangular region* of **a**

4 Conclusion

We applied surfaces with a wettability gradient fabricated with a SAM technique as a platform for spontaneous transport and coalescence of droplets. A droplet moving along the gradient surface struck another droplet on the hydrophilic region. We utilized μPIV and μLIF techniques to investigate the flow fields inside the coalesced droplets and the variation of the mixing pattern and quality of the coalesced droplet. As commonly used biochemical reagents have surface tensions that vary over a wide range, we analyzed the droplet coalescence and mixing behavior of the fluids with identical and distinct surface tension on the unclosed surface.

The mixing patterns coincide with the flow field inside the coalesced droplet. The flow mixing after the droplet coalescence also divided into two parts, one dominated by convection and the other by diffusion. For the collision of droplets with identical surface tension (cases A and B), the surface tension affects the coalescence behavior. For droplets with large surface tension (78.28 mN $\times$ m^{-1}), the large surface Gibbs energy induced a symmetric recirculation flow inside the coalesced droplet, and showed a mushroom-shaped mixing pattern inside the coalesced droplet that enlarged the material interfaces and enhanced mixing. For droplets with a small surface tension (38.63 mN $\times$ m^{-1}), the moving droplet failed to penetrate into the stationary droplet because of the small surface Gibbs energy difference before and after collision. For the collision of droplets with distinct surface tension (cases C and D), the coalescence behavior and mixing quality depend on the arrangement of the stationary and moving droplets. The stationary droplet with a larger surface tension colliding with the moving droplet with a smaller surface tension activated a mushroom-shaped mixing pattern inside the coalesced droplet, which is complementary to that for case A; The mushroom-shaped mixing pattern induced by the recirculation flow inside the coalesced droplet significantly enhanced mixing in both convection- and diffusion-dominated processes. The stationary droplet with a smaller surface tension collided with a moving droplet with a larger surface tension induced a mixing pattern of round-head shape inside the coalesced droplet, which was insufficient to enhance mixing in the diffusion-dominated mixing.

For all experimental cases, the results showed that more than 60 % of the mixing was achieved in the convection-dominated part; the mixing quality was determined within 100 ms after the droplet coalescence. The recirculation flow not only enhanced the convection-dominated mixing but also increased the rate of diffusion by enlarging the interface between the two fluids. The generation of a recirculation flow inside the coalescing droplet by surface tension or other methods is an important issue for the biological use of droplet-based micro systems. In sum, the surface tension of the stationary droplet crucially influences the convection- and diffusion-dominated mixing of droplets whereas the surface tension of the moving droplet has a slight impact on the mixing behavior and quality of droplets. The stationary droplet with a large surface tension collided with the moving droplet with a large and a small surface tension both showed the similar mushroom-shaped mixing pattern inside the coalesced droplet; the mixing indices of these two cases exceeded 0.8 at 120 s after droplet collision. The coalescence behavior and mixing quality are significantly concerned with the arrangement and configuration of different droplets on a droplet-based microfluidic system. This work significantly contributes to the understanding of droplet mixing and reaction in droplet-based microfluidic systems.

Acknowledgments National Science Council of Taiwan, ROC supported this work under grant number NSC-100-2120-M-002-013.

References

Baviere R, Boutet J, Fouillet Y (2008) Dynamics of droplet transport induced by electrowetting actuation. Microfluid Nanofluidics 4(4):287–294. doi:10.1007/s10404-007-0173-4

Blanchette F, Messio L, Bush JWM (2009) The influence of surface tension gradients on drop coalescence. Phys Fluid 21(7). doi:10.1063/1.3177339

Castrejon-Pita JR, Betton ES, Kubiak KJ, Wilson MCT, Hutchings IM (2011) The dynamics of the impact and coalescence of droplets on a solid surface. Biomicrofluidics 5(1). doi:10.1063/1.3567099

Chaudhury MK, Whitesides GM (1992) How to make water run uphill. Science 256(5063):1539–1541

Chesters AK (1991) The modeling of coalescence processes in fluid liquid dispersions—a review of current understanding. Chem Eng Res Des 69(4):259–270

Cho SK, Moon HJ, Kim CJ (2003) Creating, transporting, cutting, and merging liquid droplets by electrowetting-based actuation for digital microfluidic circuits. J Microelectromechanical Syst 12(1):70–80. doi:10.1109/jmems.2002.807467

Choi S, Jamshidi A, Seok TJ, Wu MC, Zohdi TI, Pisano AP (2012) Fast, high-throughput creation of size-tunable micro/nanoparticle clusters via evaporative self-assembly in picoliter-scale droplets of particle suspension. Langmuir 28(6):3102–3111. doi:10.1021/la204362s

Danov KD, Denkov ND, Petsev DN, Ivanov IB, Borwankar R (1993) Coalescence dynamics of deformable brownian emulsion droplets. Langmuir 9(7):1731–1740. doi:10.1021/la00031a021

Darhuber AA, Valentino JP, Troian SM, Wagner S (2003) Thermocapillary actuation of droplets on chemically patterned surfaces by programmable microheater arrays. J Microelectromechanical Syst 12(6):873–879. doi:10.1109/jmems.2003.820267

Eggers J, Lister JR, Stone HA (1999) Coalescence of liquid drops. J Fluid Mech 401:293–310. doi:10.1017/s002211209900662x

Fair RB (2007) Digital microfluidics: is a true lab-on-a-chip possible? Microfluid Nanofluidics 3(3):245–281. doi:10.1007/s10404-007-0161-8

Fang W-F, Yang J-T (2009) A novel microreactor with 3D rotating flow to boost fluid reaction and mixing of viscous fluids. Sens Actuators B Chem 140(2):629–642. doi:10.1016/j.snb.2009.05.007

Fouillet Y, Jary D, Chabrol C, Claustre P, Peponnet C (2008) Digital microfluidic design and optimization of classic and new fluidic functions for lab on a chip systems. Microfluid Nanofluidics 4(3):159–165. doi:10.1007/s10404-007-0164-5

Hosokawa K, Fujii T, Endo I (1999) Handling of picoliter liquid samples in a poly(dimethylsiloxane)-based microfluidic device. Anal Chem 71(20):4781–4785. doi:10.1021/ac990571d

Huebner A, Sharma S, Srisa-Art M, Hollfelder F, Edel JB, deMello AJ (2008) Microdroplets: a sea of applications? Lab Chip 8(8):1244–1254. doi:10.1039/b806405a

Ichimura K, Oh SK, Nakagawa M (2000) Light-driven motion of liquids on a photoresponsive surface. Science 288(5471):1624–1626

Jose BM, Cubaud T (2012) Droplet arrangement and coalescence in diverging/converging microchannels. Microfluid Nanofluidics 12(5):687–696. doi:10.1007/s10404-011-0909-z

Kapur N, Gaskell PH (2007) Morphology and dynamics of droplet coalescence on a surface. Phys Rev E 75(5). doi:10.1103/PhysRevE.75.056315

Kim J, Longmire EK (2009) Investigation of binary drop rebound and coalescence in liquids using dual-field PIV technique. Exp Fluids 47(2):263–278. doi:10.1007/s00348-009-0659-9

Kinoshita H, Kaneda S, Fujii T, Oshima M (2007) Three-dimensional measurement and visualization of internal flow of a moving droplet using confocal micro-PIV. Lab Chip 7(3):338–346. doi:10.1039/b617391h

Lai Y-H, Hsu M-H, Yang J-T (2010a) Enhanced mixing of droplets during coalescence on a surface with a wettability gradient. Lab Chip 10(22):3149–3156. doi:10.1039/c003729j

Lai Y-H, Yang J-T, Shieh D-B (2010b) A microchip fabricated with a vapor-diffusion self-assembled-monolayer method to transport droplets across superhydrophobic to hydrophilic surfaces. Lab Chip 10(4):499–504. doi:10.1039/b917624a

Lu J, Corvalan CM (2012) Coalescence of viscous drops with surfactants. Chem Eng Sci 78:9–13. doi:10.1016/j.ces.2012.04.030

Lu HW, Bottausci F, Fowler JD, Bertozzi AL, Meinhart C, Kim CJ (2008) A study of EWOD-driven droplets by PIV investigation. Lab Chip 8(3):456–461. doi:10.1039/b717141b

Orme M (1997) Experiments on droplet collisions, bounce, coalescence and disruption. Prog Energy Combust Sci 23(1):65–79

Ortiz-Duenas C, Kim J, Longmire EK (2010) Investigation of liquid–liquid drop coalescence using tomographic PIV. Exp Fluids 49(1):111–129. doi:10.1007/s00348-009-0810-7

Paik P, Pamula VK, Pollack MG, Fair RB (2003) Electrowetting-based droplet mixers for microfluidic systems. Lab Chip 3(1):28–33. doi:10.1039/b210825a

Ruardy TG, Schakenraad JM, vanderMei HC, Busscher HJ (1997) Preparation and characterization of chemical gradient surfaces and their application for the study of cellular interaction phenomena. Surf Sci Rep 29(1):3–30. doi:10.1016/s0167-5729(97)00008-3

Sellier M, Trelluyer E (2009) Modeling the coalescence of sessile droplets. Biomicrofluidics 3(2). doi:10.1063/1.3154552

Stroock AD, Dertinger SKW, Ajdari A, Mezic I, Stone HA, Whitesides GM (2002) Chaotic mixer for microchannels. Science 295(5555):647–651. doi:10.1126/science.1066238

Ting S-C, Yang J-T (2009) Extracting energetically dominant flow features in a complicated fish wake using singular-value decomposition. Phys Fluid 21(4). doi:10.1063/1.3122802

Tung KY, Li CC, Yang JT (2009) Mixing and hydrodynamic analysis of a droplet in a planar serpentine micromixer. Microfluid Nanofluidics 7(4):545–557. doi:10.1007/s10404-009-0415-8

Wang C, Nguyen NT, Wong TN (2007) Optical measurement of flow field and concentration field inside a moving nanoliter droplet. Sens Actuators A Phys 133(2):317–322. doi:10.1016/j.sna.2006.06.026

Yang JT, Chen JC, Huang KJ, Yeh JA (2006) Droplet manipulation on a hydrophobic textured surface with roughened patterns. J Microelectromechanical Syst 15(3):697–707. doi:10.1109/jmems.2006.876791

Yang ZH, Chiu CY, Yang JT, Yeh JA (2009) Investigation and application of an ultrahydrophobic hybrid-structured surface with anti-sticking character. J Micromech Microeng 19(8). doi:10.1088/0960-1317/19/8/085022